



Full Text View

[Volume 32, Issue 8 \(August 2002\)](#)
Journal of Physical Oceanography

 Article: pp. 2257–2276 | [Abstract](#) | [PDF \(3.17M\)](#)

Wind Stress Effects on Subsurface Pathways from the Subtropical to Tropical Atlantic

Tomoko Inui
Department of Earth, Atmospheric, and Planetary Sciences, Massachusetts Institute of Technology, Cambridge, Massachusetts
Alban Lazar
Earth System Science Interdisciplinary Center, University of Maryland at College Park, College Park, Maryland
Paola Malanotte-Rizzoli
Department of Earth, Atmospheric, and Planetary Sciences, Massachusetts Institute of Technology, Cambridge, Massachusetts
Antonio Busalacchi
Earth System Science Interdisciplinary Center, University of Maryland at College Park, College Park, Maryland

(Manuscript received April 25, 2000, in final form November 26, 2001)

DOI: 10.1175/1520-0485(2002)032<2257:WSEOSP>2.0.CO;2

ABSTRACT

A reduced-gravity, primitive equation, upper-ocean GCM is used to study subduction pathways in the Atlantic subtropical and tropical gyres. In order to compare the different responses in the pathways to strong and weak wind stress forcings, Hellerman and Rosenstein (HR) and da Silva (DSV) climatological annual-mean and monthly wind stress forcings are used to force the model. It is shown that subtropical–tropical communication is dependent on both the strength and structure of the wind forcing. A comparison between the two experiments shows two results for the North Atlantic: 1) the full communication window between the subtropical and tropical gyres is similar in width despite the difference in the intensity of the winds and 2) the interior exchange window width is substantially larger in the weak forcing experiment (DSV) than the strong forcing experiment (HR), accompanied by a larger transport as well. The South Atlantic exhibits a similar communication between the subtropics and Tropics in both cases. The annual-mean of the seasonally varying forcing also supports these results. A two-layer ventilated thermocline model is developed with a zonally varying, even though idealized, wind stress in the North Atlantic, which includes the upward Ekman pumping region absent from the classical ventilated thermocline model. The model shows that the communication window for subduction

Table of Contents:

- [Introduction](#)
- [Model description](#)
- [Subtropical–tropical](#)
- [Comparison with seasonally](#)
- [Exchange pathway mechanism](#)
- [Summary and conclusions](#)
- [REFERENCES](#)
- [APPENDIX](#)
- [FIGURES](#)

Options:

- [Create Reference](#)
- [Email this Article](#)
- [Add to MyArchive](#)
- [Search AMS Glossary](#)

Search CrossRef for:

- [Articles Citing This Article](#)

Search Google Scholar for:

- [Tomoko Inui](#)
- [Alban Lazar](#)
- [Paola Malanotte-Rizzoli](#)
- [Antonio Busalacchi](#)

pathways is a function of the zonal gradient of the Ekman pumping velocity, not the Ekman pumping itself, at outcrop lines and at the boundary between the subtropical and tropical gyres. This solution is validated using three additional GCM experiments. It is shown that the communication windows are primarily explained by the ventilated thermocline model without considering the buoyancy effects. From the GCM experiments, the interior exchange window, which is a part of the communication window and cannot be explained by the ventilated thermocline model, is widened by two factors: 1) eliminating part of the positive Ekman pumping region in the eastern North Atlantic and 2) weakening the Ekman pumping over the whole region. The implications of these results suggest that changes in the wind forcing on the order of the difference in the wind products used here can have a significant effect on the attributes of the communication window and, hence, the thermocline structure at lower latitudes.

1. Introduction

The interactions between the Tropics and the subtropics have only recently received significant attention, as studies have typically focused separately on either the subtropical or equatorial ocean circulations. Subtropical–tropical interactions have been investigated mostly in the Pacific, where there is well-established observational evidence of flow of thermocline water from the subtropics to Tropics. [Wyrki and Kilonsky \(1984\)](#) show that the core of the equatorial undercurrent (EUC) lies between 15° and 25°C, implying that the source region for this water is between latitudes 20° and 40° in both hemispheres, where these isotherms outcrop. Western boundary sources ([Tsuchiya 1981](#); [Lindstorm et al. 1987](#); [Tsuchiya et al. 1989](#); [Butt and Lindstrom 1994](#)) supply ~ 13 Sv ($\text{Sv} \equiv 10^6 \text{ m}^3 \text{ s}^{-1}$) to the EUC. By the time the EUC crosses $\sim 153^\circ\text{W}$ in the central Pacific it carries ~ 25 Sv of extratropical water eastward. The path this subtropical water takes to the equator is still controversial, and especially controversial is the existence of an interior pathway. Evidence of the latter was first provided by [Wyrki \(1975\)](#), who showed that some geostrophic streamlines from the North Pacific intersect the equator in the basin interior after following a “zig zag” pattern determined by the westward North Equatorial Current (NEC) and by the eastward North Equatorial Countercurrent (NECC). Even more striking is the evidence presented by [Fine et al. \(1981\)](#) and [Fine \(1987\)](#), who demonstrate the presence of a persistent subsurface tritium maximum centered on the equator between 145° and 135°W. They conclude that high tritium subtropical source waters are transported equatorward by interior geostrophic flow.

The observational evidence for subtropical–tropical exchanges in the Atlantic is more ambiguous. The Atlantic circulation is much more complex than the Pacific due to the presence of the meridional overturning cell (MOC) driven by the polar convection regions in the Norwegian/Labrador Seas, where North Atlantic Deep Water is formed. The evidence provided by tracer distributions shows a pattern very different from the one observed in the Pacific. In the Atlantic, the tritium distribution on the $\sigma_\theta = 26.80$ isopycnal surface, near the base of the thermocline and above the Antarctic Intermediate Water (AAIW), shows a band of depressed tritium values between 10° and 20°N separating the northern tritium-rich waters from the southern depleted ones. The Atlantic EUC core lies in the same temperature range as that in the Pacific, 14°–25°C ([Düing et al. 1980](#)), corresponding to a range in σ_θ of 24.5–26.8 ([Frantantoni 1996](#); [Frantantoni et al. 2000](#)), indicating that the source regions for these waters lie in the subtropics. Most of the water in the EUC seems, however, to be of South Atlantic origin ([Metcalf and Stalcup 1967](#); [Wilson et al. 1994](#)).

On the theoretical side, the first investigation of the dynamical connections between the tropics and the subtropics was carried out by [Pedlosky \(1987\)](#) as an equatorial extension of the ventilated thermocline theory ([Luyten et al. 1983](#), hereafter LPS). The intriguing aspect of this theory is that the EUC and equatorial upwelling are remotely driven by subtropical subduction with the equatorial upwelling adjusting to absorb all the EUC transport. The theory thus provides an alternative to the “classical” explanation of the EUC being primarily driven by the equatorial wind field. The theory was subsequently extended by explicitly including the different dynamical regimes that connect the subtropics to the equator both in analytical studies ([McCreary and Lu 1994](#); [Liu 1994](#)) and in numerical ones ([McCreary and Lu 1994](#); [Liu et al. 1994](#); [Lu and McCreary 1995](#); [Liu and Philander 1995](#); [Blanke and Raynaud 1997](#); [Rothstein et al. 1998](#); [Lu et al. 1998](#)).

Some of the numerical studies even provide contrasting results; see for instance, the numerical investigation of [Lu and McCreary \(1995\)](#) with a reduced-gravity two-layer model and investigations carried out with fully three-dimensional general circulation models (GCMs) by [Liu et al. \(1994\)](#), [Liu and Philander \(1995\)](#), [Blanke and Raynaud \(1997\)](#), and [Rothstein et al. \(1998\)](#). In the [Lu et al. \(1988\)](#) and [Lu and McCreary \(1995\)](#) work, water masses subducted in the subtropics must flow to the western boundary before turning equatorward in a western boundary current to join the EUC at the equator.

By and large, all of the above studies have focused on the Pacific. To our knowledge, the only numerical investigations carried out for the Atlantic are those by [Frantantoni \(1996\)](#), [Frantantoni et al. \(2000\)](#), [Harper \(2000\)](#), [Blanke et al. \(1999\)](#), [Malanotte-Rizzoli et al. \(2000\)](#), and [Lazar et al. \(2001a,b\)](#). [Frantantoni's \(1996\)](#) study focuses on the total transport of mass from one gyre to another and the modifications induced in this total transport by superimposing the MOC on the wind-driven circulation. In Harper's study, particle trajectories indicate that the subducted water reaching the EUC comes exclusively from the southern subtropics. [Malanotte-Rizzoli et al. \(2000\)](#) show that surface waters in 20°–22°N and 6°–15°S reach the equatorial region in the Atlantic.


The conceptual framework that has emerged from this body of research has led to the definition of four windows in the subtropics. The first one is the “recirculation window” in which fluid parcels subducted in the western subtropics at latitudes between 15° and 30°N recirculate within the subtropical gyres both in the Northern and Southern Hemispheres. The second pathway originates in the central subtropics where subducted particles flow first to the western boundary, then turn equatorward and are entrained into the EUC at the equator—this is the “western boundary exchange window.” The third pathway reaches the equator and the EUC in the basin interior far from the western boundary—this is the “interior exchange window.” The final pathway is the “island circulation” that flows equatorward first and eventually goes back (a closed cyclonic circulation) in the eastern part of the basin. We will examine the two exchange windows (i.e., western boundary and interior exchange windows) and the island circulation since these regions have interactions between the subtropics and the Tropics. Also, we define a communication window that consists of the two exchange windows.

In the GCM simulations both in the Atlantic and Pacific, there is a well-defined, unambiguous interior pathway from the subtropics to the equator. Those previous studies showed various widths of each window without a full explanation. [Liu \(1994\)](#) used a LPS-type model driven by zonally uniform winds, with a zonally uniform negative Ekman pumping, to explain the width of the communication window as a function of Ekman pumping velocity at the gyre boundary and the outcrop line. However, the North Atlantic has a large region of positive Ekman pumping that is not negligible, to which his solution does not apply. Therefore, the major objective of this paper is to investigate and explore the sensitivity of the above scenario, especially the presence or absence of the interior exchange window from which tracers or temperature anomalies propagate without changing their properties to the surface forcings. Wind stress, heat, and moisture fluxes will be used in numerical simulations for the Atlantic to study such dependencies. We will use a modified LPS model as well. The basin is characterized by a strong intertropical convergence zone (ITCZ) that has important seasonal fluctuations, being located between 0° and 10°N in winter but shifting to 10°–20°N and intensifying in summer. The ITCZ induces a pool of surface Ekman upwelling that may constitute a potential vorticity barrier, deflecting subducted parcels to the western boundary. A further major objective is to assess how the water mass pathways diagnosed from the calculation forced by steady winds are representative of the pathways obtained by including the seasonal cycle of the wind stress, and hence to what extent can they be used as predictors for the seasonally varying circulation.

The paper is organized as follows. In [section 2](#) a brief description is provided of the model, the forcing functions, and the experiments. In [section 3](#) the Atlantic subtropical/tropical circulation obtained with steady wind stress forcing is analyzed. Water mass pathways are diagnosed first by comparing the Bernoulli function associated with specific isopycnal surfaces (which is the streamfunction for an adiabatic ocean). A trajectory analysis is also carried out by injecting Lagrangian floats onto isopycnals of interest (i.e., the isopycnals bounding the upper equatorial thermocline, both in the Northern and Southern Hemispheres). In [section 4](#), we compare the water mass pathways predicted by the steady wind forcing with those diagnosed in the simulation with seasonally varying winds. In [section 5](#), we explore mechanisms determining the interior pathway in the North Atlantic, using a steady-state analytical calculation based on the LPS theory. Finally, in [section 6](#), we present the conclusions of the research and possible directions for future work.


2. Model description

A reduced-gravity, primitive equation, sigma-coordinate OGCM ([Gent and Cane 1989](#); [Murtugudde et al. 1996](#)) with the embedded hybrid mixing scheme of [Chen et al. \(1994\)](#) is employed to simulate the Atlantic circulation. The model was used previously to study subduction in the North Pacific by [Rothstein et al. \(1998\)](#). The model explicitly accounts for a complete upper ocean hydrology ([Murtugudde and Busalacchi 1998](#)) with freshwater fluxes treated as a natural boundary condition ([Huang 1993](#)). This model is also coupled to an atmospheric mixed layer model ([Seager et al. 1995](#)), which calculates 1) net heat flux that requires inputs of solar radiation (ERBE), cloud cover (ISCCP), precipitation (P) ([Oberhuber 1988](#)) and winds; and 2) evaporation (E), which will be used to calculate the freshwater flux ($E - P$). Therefore, there is no explicit relaxation to a prescribed sea surface temperature so comparison with a climatology ([Levitus 1982](#)) is necessary to evaluate the model performance. There is no flux correction term and salinity is forced by the freshwater flux ($E - P$).

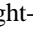
The model domain is 50°N–50°S, 100°W–20°E ([Fig. 1](#) ) with Ekman pumping fields evaluated from climatological mean wind stress curl fields. Horizontal resolution is $0.5^\circ \times 0.5^\circ$. The vertical structure of the model ocean consists of a mixed layer and a specified number of layers below. The mixed layer depth and the last sigma layer are computed prognostically. The remaining layers are computed diagnostically such that the ratio of each sigma layer thickness to the total layer thickness remains fixed to a prescribed value. Twenty sigma layers are used and the mean sigma-layer thickness in the outcropping region of the North Atlantic subtropical–tropical circulation are 14.2 m (layers 2–5), 28.4 m (layers 6–9), 56.7 m (layers 10–13), 85.1 m (layers 14–15), 142.0 m (layers 16–17), 280.0 m (layer 18), and 420.3 m (layers 19–20). The bottom layer is set to be $\sigma_\theta = 27.8$ (kg m^{-3} , hereafter, the unit is not used). This isopycnal lies about 2000 m deep.

The hybrid vertical mixing scheme for the mixed layer combines the traditional bulk formulae of [Kraus and Turner \(1967\)](#) with the dynamic instability model of [Price et al. \(1986\)](#). This allows the inclusion of three major processes of oceanic vertical mixing: 1) the bulk mixed layer model, which relates the mixed layer entrainment/detrainment to the atmospheric forcing; 2) the gradient Richardson number mixing, which accounts for shear flow instability; and 3) a convective adjustment which simulates the high-frequency convection.

The reduced-gravity model could underestimate the northward return flow caused by the meridional overturning circulation since the deeper part of the ocean is not included in the model. However, this issue is partially addressed by restoring temperature, salinity, and the layer thickness toward their observed vertical profiles at the open boundaries. The model ocean is initially at rest with initial temperature, salinity, and layer thicknesses taken from the [Levitus \(1982\)](#) annual

mean data. The annual mean of the temperature, salinity, and the layer thickness from [Levitus \(1982\)](#) climatology is used to restore the northern and southern boundaries (within 5°) in annual-mean experiments. For seasonally varying experiments, the monthly temperature, salinity, and layer thickness from [Levitus \(1982\)](#) are used to restore the northern and southern boundaries. These sponge-layer boundary conditions thus mimic the flow to the North Atlantic from the Arctic Ocean and the mass exchange between the South Atlantic and the Antarctic polar ocean. The model is driven by the seasonally varying and annual means of [da Silva et al. \(1994\)](#) and [Hellerman and Rosenstein \(1983\)](#) 1) wind stress fields, 2) heat fluxes, and 3) freshwater flux ($E - P$), calculated in the atmospheric mixed layer model ([Seager et al. 1995](#)). Ekman pumping velocity fields outside of the equatorial region (excluding the region between 5°N and 5°S) for both wind stress datasets are shown in [Fig. 1](#) , calculated as

$$w_e = \frac{1}{\rho} \text{curl} \left(\frac{\tau}{f} \right) = \frac{1}{\rho f} \left(\text{curl}(\tau) + \frac{\beta \tau^x}{f} \right) \quad (1)$$

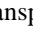
where the wind stress is $\tau = (\tau^x, \tau^y)$, the Coriolis parameter is f , atmospheric density is ρ , and $\beta = \partial f / \partial y$. The second term on the right-hand side causes downwelling, even in the equatorial gyre (bounded by the thick dashed lines in [Fig. 1](#) ) , that allows water communication from the surface to the interior ocean through the subduction process. The model is integrated for over 50 years in each experiment until it reaches a reasonable equilibrium state both for the seasonally varying and the annual mean experiments.


3. Subtropical–tropical circulation in the Atlantic

In this section we describe the results for experiments driven by steady annual mean forcings. Experiments driven by the [da Silva et al. \(1994\)](#) wind stress are referred to as DSV experiments, and those driven by the [Hellerman and Rosenstein \(1993\)](#) wind stress are referred to as HR experiments. The major difference between these two wind stress products is that DSV is weaker and HR is stronger in the subtropical–tropical gyres, although both experiments show a reasonable model SST field.


The vertically integrated meridional transport stream function is calculated according to

$$\psi(x, y) = \int_x^{x_e} \int_{z=z_m}^{z=\text{bottom}} v(x, y, z) dz dx, \quad (2)$$

where the bottom is taken to be the depth of the $\sigma_\theta = 27.8$ surface, z_m is the mixed layer depth, v is the meridional velocity, and x_e is the eastern boundary of the basin. The subduction process and the mixed layer process involve different physics, and we want to assess how much of the water is transported into the equatorial region through the thermocline. These transports are shown in [Fig. 2](#) . Due to the stronger HR wind stress compared to DSV wind stress, 1) the transport in the HR subtropical gyre is larger and 2) the subtropical and equatorial regions in the HR North Atlantic are separated by a rather strong cyclonic equatorial gyre centered at 10°N . This difference is particularly evident in the region of the model North Brazil Current. In the South Atlantic, the equatorial circulation is similar for both forcings.

The thermocline structure at 10°N is more tilted in the east–west direction for the stronger forcing experiment (HR), indicating a stronger current system. The equatorial thermocline structure along 10°N and the equator is examined to identify which isopycnal surfaces bound the thermocline for the strong and weak forcing experiments ([Fig. 3](#) ). The upper equatorial thermocline is bounded approximately by $\sigma_\theta = 24.0$ – 25.0 in the strong forcing experiment (HR) and by $\sigma_\theta = 24.5$ – 25.0 in the weak forcing experiment (DSV). The lower bounds are approximately the largest density range where the subtropical thermocline water flows into the equatorial thermocline without reaching the western boundary. The latitude of the outcrop lines of these bounding isopycnals is similar in both experiments; thus it is appropriate to analyze results with respect to different bounding isopycnals in each experiment and the thermocline structure at 10°N because the outcrop lines of the bounding isopycnals are located approximately within 10° and 15°N .

a. The Bernoulli function

In the context of a general depiction of the flow field, it is useful to interpret all the results in terms of adiabatic, inviscid dynamics in which water parcels move along isopycnal surfaces. Pathways are diagnosed on several isopycnal surfaces using the Bernoulli function. The isopycnals of interest were determined from the thermocline structure ([Fig. 3](#) ) in order to assess water pathways from the subtropical to the tropical gyres.

The Bernoulli function, B , on an isopycnal is defined as

$$B(a) = P_0 + \int_{z=z(a)}^{z=\text{surface}} g[\sigma_\theta - a] dz + \frac{1}{2} \rho_0 (\mathbf{u}_a)^2, \quad (3)$$

where $\sigma_\theta = a$ is the isopycnal surface of interest and \mathbf{u}_a is the current vector on the isopycnal surface of $\sigma_\theta = a$; $P_0 = \rho_0 g \eta$ in which $\rho_0 = 1020.0 \text{ g cm}^{-3}$ and η is the sea surface elevation. This is the definition of the pressure (i.e., the Bernoulli function) on an isopycnal surface for a steady and incompressible flow (Welander 1971). Note that σ_θ does not correspond to the model sigma layer since the former is an isopycnal and the latter is a layer that is determined as a prescribed ratio to the total layer thickness.

Flow fields on the isopycnals of ($\sigma_\theta = 24.5, 25.0, 25.5$) for the weak forcing experiment (DSV) are shown in Fig. 4 with current vectors superimposed. First, the general features will be described using the result from this experiment. The “island” of closed streamlines (the shaded region) is induced by the region of positive Ekman pumping (Fig. 1), which is located in the eastern basin between 10° and 20°N in the North Atlantic. However, the shaded regions extend west of the region of positive Ekman pumping because the western end of the island is determined by the condition $\int_x^{\text{eastern}} w_e dx = 0$, which is different from the line of $w_e = 0$. The interior pathways that define the interior exchange window (marked on the figures) emanate from the outcrop lines through the equatorial region, which start at $\sim 40^\circ\text{W}$ on the $\sigma_\theta = 24.5$ isopycnal. Together with the western boundary exchange window, the communication window (the interior and western boundary windows) comprises a region of $\sim 10^\circ$ width at $\sim 15^\circ\text{N}$. On the $\sigma_\theta = 25.0$ isopycnal, the communication window is between $\sim 35^\circ\text{W}$ and 43°W at $\sim 17^\circ\text{N}$. No interior pathways exist on the deeper isopycnal $\sigma_\theta = 25.5$ (Fig. 4c). In the South Atlantic, interior pathways are clearly present on both $\sigma_\theta = 24.5$ and $\sigma_\theta = 25.0$. The western boundary exchange window is particularly evident on all three isopycnals of Fig. 4. On $\sigma_\theta = 25.0$ (Fig. 4b), the interior and western boundary windows emanate from the southern outcrop line between $\sim 10^\circ\text{E}$ and 15°W at $\sim 25^\circ\text{S}$.

The Bernoulli function on the $\sigma_\theta = 24.5$ surface for strong forcing (HR) experiment is compared to the one of the $\sigma_\theta = 25.0$ surface for weak forcing (DSV) experiment since both outcrop lines are located closely and the isopycnal depth is in a similar range. The island structure is stronger in the strong forcing (HR) experiment, which is in reasonable agreement with the Ekman pumping pattern, since the strength of the upward Ekman pumping velocity is significantly larger for the stronger wind (HR) (Fig. 1). The interior pathways from the outcrop line through the equatorial region are located west of the $\sigma_\theta = 24.5$ island, which form a narrower region than that for the $\sigma_\theta = 25.0$ of the weak forcing experiment, and no interior pathways exist on deeper isopycnals. The Bernoulli streamlines in the South Atlantic also show clear interior pathways from the outcrop lines, regardless of the intensity of the wind forcing.

Next, we demonstrate that subduction occurs in the subtropical gyre in both hemispheres corresponding to the interior and western boundary exchange windows, where Bernoulli isolines emanate from the outcropping lines of the isopycnals to the equatorial thermocline. Following Cushman-Roisin (1987), the instantaneous subduction rate is given by

$$S(t) = \frac{dh}{dt} - \left[\frac{d(hu)}{dx} + \frac{d(hv)}{dy} \right] \quad (4)$$


with h the mixed layer depth and (u, v) the mixed layer currents. Since our simulation is stationary, the first term on the right-hand side of Eq. (4) is zero and the annual subduction rate is simply the constant divergence of the mixed layer horizontal flow integrated over one year. Figure 6 displays this quantity for the strong forcing (HR) experiment. Two regions are relevant for the present analysis in the pattern of the annual subduction rate. First, in the northwestern Tropics, there is a broad subduction region with an annual rate of the order of 50 m yr^{-1} confined between $\sim 35^\circ$ and $\sim 48^\circ\text{W}$ centered at $\sim 15^\circ\text{N}$. This subduction region corresponds well to the region of the North Atlantic communication window (interior + western boundary) found on $\sigma_\theta = 24.5$ in Fig. 5. In the South Atlantic, there is a broad subduction region between 15° and 30°S , 20°W and $\sim 5^\circ\text{E}$. This subduction region corresponds well to the communication window originating from the outcropping line of $\sigma_\theta = 24.5$ in the South Atlantic in Fig. 5. Note that the broad patterns of this subduction rate compare well to those computed for a climatological seasonal cycle of the same model configuration (Lazar et al. 2001a).


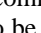
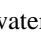
We comment now about the realism of the model simulations and how adequately they reproduce the zero-order features of the Atlantic subtropical and tropical circulations. We carry out comparisons between our Bernoulli functions on different isopycnal surfaces and the dynamic heights evaluated by Zhang et al. (2002, manuscript submitted to *J. Phys. Oceanogr.*) on the same isopycnals from the Atlantic climatological hydrography. (We are unable to show their results as they are part of a manuscript in preparation.) Suffice to say that the Bernoulli patterns obtained in the DSV experiments, shown in Fig. 4, compare extremely well with the dynamic heights on the same isopycnals both in the northern and southern Atlantic. This comparison gives us confidence that the exchange transports and window sizes evaluated in the numerical experiments in this study indeed provide realistic estimates for the mean circulation.

b. Trajectory analysis

To confirm the above results, a Lagrangian trajectory analysis was carried out using the mean current data projected onto

isopycnal surfaces. Particles are released beneath the mixed layer along outcrop lines to identify regions of communication between the subtropics and Tropics. We do not show the trajectories of this consistency check as they confirm the patterns provided by the Bernoulli function fields.

The boundaries of the recirculation/western boundary/interior/island windows along the outcrop lines of the upper equatorial thermocline isopycnals are shown in [Fig. 6](#)  for the density surface lying in the same depth range and outcropping in the same latitude range. The strong forcing experiment (HR) shows a smaller interior exchange window than for the weak forcing experiment (DSV), although both isopycnal lines of $\sigma_\theta = 24.5$ (HR) and $\sigma_\theta = 25.0$ (DSV) are at similar locations. In a similar way, the interior exchange window is smaller on $\sigma_\theta = 24.0$ for the strong forcing (HR) experiment than on $\sigma_\theta = 24.5$ for the weak forcing (DSV) experiment. The interior exchange windows (marked with circles) are wider for weak forcing (DSV), implying that the equatorial region is ventilated by a wider area in longitude in the subtropical gyre, independently from the actual transport.

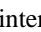
Both the Bernoulli function diagnostics and the Lagrangian trajectory analysis are carried out by projecting the current velocities onto isopycnal surfaces, thus not accounting for possible diapycnal flow. These diagnostics are meant to be only qualitative, and not aimed at quantifying water mass transformations as in [Blanke et al. \(1999\)](#). We point out, however, that the Bernoulli function provides information about possible diapycnal flows that can be calculated by using horizontal velocities and the convergence of the water. The Bernoulli function is the streamfunction of adiabatic flow. Therefore, in regions where the velocity vectors are parallel to the Bernoulli isolines, the flow occurs on isopycnal surfaces, and the diapycnal component is negligible. Examination of [Figs. 4](#)  and [5](#)  shows that indeed the interior flow in the North Atlantic, and particularly the flow subducting in the communication windows and ventilating the equatorial thermocline, is parallel to the velocity vectors and thus very likely to be adiabatic with respect to this pathway diagnostic. Regions where the velocity vectors cross the Bernoulli isolines are mostly located near the western boundary, along the equator and, less significantly, in the eastern upwelling regions. An interior region where the Bernoulli diagnostic suggests interior diapycnal fluxes, with significant crossing of velocity vectors and isolines, is centered near 10°S , 5°W within the Angola gyre, below the tropical upwelling seen in [Fig. 7](#) . Therefore, water mass transformations in the model occur only in these areas and not in the exchange window regions located in the eastern part of the basin.

c. Transport analysis

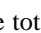
The meridional transport streamfunction is calculated according to

$$\psi(x, y) = \int_x^{x_e} \int_{z=\sigma_{\theta 1}}^{z=\sigma_{\theta 2}} v(x, y, z) dz dx \quad (5)$$

where v is the meridional velocity, and $\sigma_{\theta 1}$ and $\sigma_{\theta 2}$ are the two bounding isopycnals. Since the focus of this paper is on the subsurface pathways, transports are calculated for the waters that have already been subducted from the mixed layer into the subtropical thermocline. The transport streamfunction is evaluated from the second layer to the last layer of the reduced-gravity model, not including the mixed layer. The thermocline transport streamfunction is calculated between the bounding isopycnals and constitutes the transport to the equatorial thermocline from the subtropical gyre.

We examined the sensitivity of the transport estimates to the choice of the bounding isopycnals, repeating the analysis for a wide range of densities with a $0.1 \sigma_\theta$ interval. Then, we chose the two bounding isopycnals to quantify the subduction process in a layer scenario. The deepest bounding surface chosen is the one where the interior pathway disappears. As an example, in the weak forcing (DSV) experiment, no interior pathway is present on the $\sigma_\theta = 25.5$ isopycnal ([Fig. 4c](#) ) , and $\sigma_\theta = 25.2$ was the deepest bounding surface. The upper bounding surface is chosen to be the one outcropping north of 10°N where the subduction process is not affected by strong seasonal variability in the North Equatorial Current. The transports were then evaluated with the fine σ_θ interval, which however did not change the ratio of the transport of the different exchange windows significantly, as compared to the calculation with only two bounding isopycnal surfaces. Only a more detailed description with unchanged overall transports is provided by the fine-interval calculation.

Transports between the two isopycnals are evaluated at 10°N (close to the gyre boundary between the subtropical and equatorial gyres) for the three windows (out of four) that interact with the Tropics: the western boundary, interior, and island regions. Here 10°N was chosen because the positive Ekman pumping extends farthest west at this latitude as explained in the introduction, a latitude where the communication transport is expected to be the least. The entire communication window is at its zonal minimum.


[Figure 8](#)  shows four transport components: the total southward transport below the mixed layer, the western boundary exchange transport, the interior exchange transport, and the island transport. The transport within each window is not normalized; instead, the ratio to total southward transport is calculated for each of the three components and given as a percentage in the figure.



The western boundary exchange window plays a more important role for strong forcing (HR) while the interior exchange transport appears to be small. For the weak forcing (DSV), the interior exchange window transport is $\sim 1/2$ of the western

boundary exchange compared to the ratio of 1/5 for strong forcing (HR) experiment. It is shown that the thermocline transport for weak forcing (DSV) has a larger interior exchange window as well as a larger transport through it. The mechanism will be discussed in [section 5](#).



4. Comparison with seasonally varying experiments


In [section 3](#), it was seen that a weaker wind stress creates a wider interior exchange window and more transport through this window. The question arises whether this picture is still valid for the yearly averaged circulation driven by seasonally varying wind stress fields. Mean fields from seasonally varying experiments are therefore examined for possible rectification of the seasonal effects onto the annual mean fields.

Clearly, the wind stress pattern determines the westward extension of the island of closed cyclonic circulation. The seasonal variability of the wind stress shows that the zero wind stress curl line (ZWCL) moves from 10° to 20°N from February to August, and hence the positive Ekman pumping velocity (in the equatorial gyre) completely disconnects the barotropic subtropical and equatorial circulations in August ([Fig. 9](#) ). As a result, the streamlines are bent strongly westward in August at ~ 10°N, while they proceed directly to the equator in the interior in February. These results suggest that the smallness of the positive Ekman pumping region becomes a crucial factor in allowing for a communication window, at least within the seasonal timescale.

However, the annual mean from experiments forced by the seasonal climatology of the wind stresses are found to be similar to the annual mean experiments: 1) The trajectory analysis (not shown) and the Bernoulli function fields diagnosed in the yearly averaged circulations ([Fig. 10](#) ) again show that the interior exchange windows are wider for the weak forcing experiment; 2) the ratio for the western boundary exchange transport to the interior transport is again 2:1 for the weak forcing (DSV) experiment, while it is 5:1 for the strong forcing (HR) experiment (figures not shown), the same ratio as shown in the annual mean experiments ([Fig. 8](#) ). In the seasonally varying experiment, the trajectories were calculated in the fully time-dependent circulation as well as in the annual mean, and they showed little difference for the timescale of 3–5 years if the particles are released in the optimum season, when the Ekman pumping is downward ([Lazar et al. 2001a](#)). As long as the flow fields do not include mesoscale eddies, the flow of the subduction process is consistently slow ($\sim 1 \text{ cm s}^{-1}$) and is not affected significantly by the seasonal variability after the particles are subducted into the thermocline. For this reason, after the particles are subducted, the overall trajectories are similar in the fully time-dependent, the mean of the seasonally varying, and the annual-mean-averaged experiments. Therefore, results for the annual mean experiments are used to investigate the mechanisms responsible for the changes in the exchange windows and pathways in response to the wind stress fields.

5. Exchange pathway mechanism in the North Atlantic

[Liu \(1994\)](#) investigated the factors that determine the size of the subtropical–tropical communication window by comparing the results from a GCM and an idealized LPS-type model. The analytical treatment presented here follows Liu's, but with a major and important difference. Like [Liu \(1994\)](#), we consider a 2.5-layer model, that is, a model with two moving layers, in which the lower layer is the subduction layer to the equatorial region ([Fig. 11](#) ). Even though [Liu \(1994\)](#) added a surface mixed layer, he actually evaluated the condition for the lower (second) layer to ventilate into the tropics in the limit of vanishing surface layer thickness [his Eq. (4.2)], so his LPS model is the same as ours. However, [Liu \(1994\)](#) used zonally uniform winds with a zonally uniform negative Ekman pumping, and it is not obvious that such a solution may apply when there is a region of positive Ekman pumping or a zonal gradient in the wind stress curl. Regions of positive Ekman pumping, induced by the ITCZ, are observed in both the eastern tropical Pacific and Atlantic Oceans. They produce a closed cyclonic circulation, reproduced in our experiments and in [Lazar et al. \(2001a\)](#) for the Atlantic and in [Rothstein et al. \(1998\)](#) for the Pacific in realistic GCM configurations. Such a closed cyclonic circulation is also observed in the dynamic heights evaluated by [Johns et al. \(2001\)](#) from the Atlantic climatological hydrography. Thus, [Liu's \(1994\)](#) analytical treatment excluded a major feature of the eastern tropical basin around 10°–20°N in the Atlantic where an important subduction region exists, as previously shown in [Fig. 7](#) . The analytical treatment in our study includes the region of positive Ekman pumping. Thus, the major difference from [Liu's \(1994\)](#) work is that our Ekman pumping velocity is not zonally uniform but longitude dependent. We will show that the width of the “communication window” in [Liu's \(1994\)](#) terminology, which combines our western boundary and interior windows, depends on the *zonal gradient* of the Ekman pumping velocity and not on the Ekman pumping itself. This idealized prediction is confirmed by the more realistic numerical calculations at the end of this section.

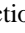

The idealized basin is shown in [Fig. 11](#) . Assumptions are made that specifically apply to low-latitude North Atlantic wind stress fields. The Ekman pumping (W_e) is assumed to be a linear function of longitude with a zonal gradient ($W_0(f)$) and zero-crossing at the longitude $x_c(f)$ (x and f represent longitude and latitudes, respectively):

$$W_e(x, f) = W_0(f)G(x, f) = W_0(f)[x - x_c(f)]. \quad (6)$$

The Ekman pumping distribution follows this approximate form between 5° and 20°N, where the North Atlantic subtropical–tropical circulation is examined in this study. The basic LPS equations are given in the appendix. We have positive Ekman pumping in the easternmost region, which induces a cyclonic gyre in the first(surface) layer. The boundary of the cyclonic gyre is determined by the line of $X\psi(f)$, where

$$\int_{x_\psi}^{\text{eastern}} W_e(x, f) dx = 0,$$

that is, where $\psi_{\text{barotropic}} = 0$. In our approximation of W_e , the Ekman pumping = 0 line, x_c , is located in the center between the eastern boundary and $X_\psi(f)$ because the integrated form of the Ekman pumping [Eq. (5)] is a quadratic form (this is simply the Sverdrup relation).

The inclusion of a positive Ekman pumping region, and of the closed cyclonic gyre, leads to an artificial assumption that the outcrop line of the subduction layer at the subduction latitude f_0 terminates at X_ψ (see Fig. 11a ) , where the outcrop line intersects the line of zero barotropic transport enclosing the cyclonic gyre. We admit this assumption to be unrealistic, but it allows derivation of a simple analytical solution that highlights the importance of the zonal gradient— $W_0(f_0)$ —of the zonal pumping velocity at the subduction latitude in determining the width of the communication window from the subtropics to the equator. Under this assumption, the easternmost characteristic emanating into the lower layer from the subduction latitude f_0 is the line x_4 (Fig. 11a ) . The Sverdrup relation can be closed within X_ψ , thus confining the interior wind-driven cyclonic circulation. Between x_4 and X_ψ the lower layer is forced neither by subduction nor by the wind, and hence is motionless. This is the shadow zone.

To derive the width of the communication window, we consider the characteristic x_2 that separates the ventilated region from the water recirculating in the subtropical gyre. Specifically, the potential vorticity at point $(0, f_d)$ is assumed equal to that at the subduction point (x_2, f_0) :

$$\begin{aligned} \frac{2f_0^2}{\gamma_2\beta} \int_{x_2}^{x_{\psi 0}} W_e(x, f_0) dx + H_0^2 \\ = \frac{2f_d^2/(\gamma_2\beta) \int_0^{x_{\psi d}} W_e(x, f_d) dx + H_0^2}{1 + (1 - f_d/f_0)^2 \gamma_1/\gamma_2}, \end{aligned} \quad (7)$$


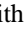
where the γ_i is the density difference between the layer i and $i + 1$. The communication window that supplies water to the equatorial region is defined as the distance from the western end of the exchange window (x_2) to the zero Sverdrup transport line ($X_\psi(f_0)$). Thus, the window can be treated roughly as the sum of the western boundary and the interior exchange windows in the GCM results. From Eq. (6), the boundary between the recirculation and western boundary windows (x_2) at the outcropping latitude f_0 is evaluated in terms of the distance from the zero Ekman pumping velocity longitude (x_c):

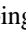
$$(x_2 - x_c(f_0))^2 = (X_{\psi 0} - x_c(f_0))^2 + \frac{\beta}{f_0^2 \mathbf{W}_0(\mathbf{f}_0)} \left[\left(\frac{f_d^2 \mathbf{W}_0(\mathbf{f}_d)}{\beta} F_1 - \gamma_2 H_0^2 \right) / F_2 + \gamma_2 H_0^2 \right]. \quad (8)$$

(Click the equation graphic to enlarge/reduce size)

Notice that subduction occurs only in the region between x_2 and X_ψ , and

$$\begin{aligned} F_1 &= 2x_c(f_d)X_{\psi d} - X_{\psi d}^2, \\ F_2 &= 1 + (1 - f_d/f_0)^2 \gamma_1/\gamma_2. \end{aligned}$$

In (8), β is the meridional gradient of the Coriolis parameter, f_d is the gyre boundary latitude between the subtropics and Tropics, $x = 0$ is the western boundary longitude, and X_ψ and $X_{\psi d}$ are the boundary of the cyclonic gyre at the outcrop and gyre boundary, respectively; H_0 is the layer thickness on X_ψ (eastern boundary of the ventilated thermocline) at the outcropping latitude. The vertical structure for the thermocline is shown in the middle and lower panels of Fig. 11  . At the outcrop latitude f_0 (middle panel of Fig. 11 ), the second layer is determined totally by the Sverdrup relation, with the closed cyclonic gyre confined to the east of X_ψ . South of the outcrop line, that is, between f_0 and f_d , there is a surface layer to the west of X_ψ , and a shadow zone exists between x_4 and X_ψ in the second layer.


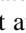

How the western edge of the communication window (x_2) changes for different wind stress forcing can be easily discerned. The western edge of the communication window at an outcrop latitude moves westward as the *zonal gradient of Ekman pumping* at the outcropping latitude $W_0(f_0)$ becomes smaller (Fig. 12 ) , while the zonal gradient of the Ekman pumping at the gyre boundary $W_0(f_d)$ remains fixed. It should be noted that x_2 is not affected by the assumption of setting $X_\psi = 0$. Since Eq. (7) is the integral of the Ekman pumping, $\int_{x_2}^{X_{\psi_0}} W_e dx = \int_{x_2}^{\text{eastern}} W_e dx$ and $\int_0^{X_{\psi_d}} W_e dx = \int_0^{\text{eastern}} W_e dx$, x_2 is not affected by the position of X_ψ or by its value.

The HR (strong) and DSV (weak) stress data have a different zonal Ekman pumping gradient, both at the outcrop and gyre boundary latitudes. The previous analytical derivation, even though highlighting the role of the zonal gradient of the Ekman pumping velocity, is too crude to fully elucidate the difference between these two experiments since the zonal gradient of the Ekman pumping velocity is small for the DSV in both latitudes. Also, the solution only predicts the position of the communication window, but not the interior exchange window whose differences were seen clearly in section 3 between the results from strong/weak forcing. For these reasons, the following three experiments were carried out with the steady annual-mean wind stress forcings, aiming to change the zonal gradient of the Ekman pumping velocity, both at the outcrop and gyre boundary latitudes (expts 1 and 3) and only at the outcrop latitude (expt 2), specifically,





1. experiment 1: Eq-20°N of DSV wind stress field
2. experiment 2: 15°-30°N of DSV wind stress field
3. experiment 3: HR used over the entire domain but intensity reduced by a factor of 0.75.


The model was integrated for 50 years until it reached a steady state. A transition region of 3° width was set at the boundaries, where the different wind stress datasets were blended to avoid a strong discontinuity.


Experiment 1 addresses the importance of the wind stress over the tropical gyre to show that simply switching to weak tropical wind stress produces a circulation pattern similar to the weak forcing (DSV) experiment of section 3. Experiment 2 demonstrates how the entire communication window changes if only the wind stress over the outcrop region is changed (the southern part of the subtropical gyre) while the wind stress at the gyre boundary latitude remains fixed. Experiment 3 demonstrates that the entire communication window is unchanged when the ratio of the zonal gradient of Ekman pumping, $W_0(f_d)/W_0(f_0)$, is not changed by reducing the wind stress. Experiment 3 also examines whether a reduced wind stress allows for more transport through the interior communication window. The value of 0.75 is obtained by taking an approximate ratio of the DSV and HR wind stress in the whole region. Thus, the Ekman pumping pattern in experiment 3 is identical to the original HR wind stress but differs in magnitude.

The trajectory analysis is carried out for each experiment as discussed in sections 3 and 4 to identify the western boundary and interior exchange windows (Fig. 13 ) . Even when the windows are wider, their transport may not be larger. Therefore, the transports at 10°N are evaluated for the equatorial thermocline layer and for the total layer below the mixed layer (Fig. 14 ) . The southward transport at 10°N carried by each exchange window is evaluated as well (Fig. 16 ) .

a. Communication window width

As specified earlier, the communication window is the sum of the western boundary and the interior exchange windows in the results from the numerical simulations. To describe the communication window by following Eq. (6), the distance between the point marked with a cross and the zero Ekman pumping velocity line is used in Fig. 3 ) . The point marked with a cross corresponds to the subducting characteristics separating the recirculation and communication windows, that is, to the characteristics x_2 in Fig. 11 ) . The ZEPL (zero Ekman pumping line), and the ZMTL (zero meridional transport function line) are calculated and marked in Fig. 13 ) to examine to what extent the circulation follows the prediction obtained from the wind stress alone. Notice that these lines are directly evaluated from the wind stress field used in each experiment. A “choke latitude” (Huang and Wang 2001), where the vertically integrated transport is expected to be minimum, is located at 10°N for each experiment. The standard case to be compared with each experiment is the HR experiment in Fig. 7a ) .

First, the effects of winds over the tropics (eq to 20°N) are discussed. The result from experiment elucidates how switching the tropical wind stress affects the pathways of the subtropical water. The communication window along the outcrop lines of the considered isopycnals becomes similar to that of the DSV experiment rather than to those of the HR experiment (Fig. 13a ) .

Second, in experiment 2, the zonal gradient of the Ekman pumping is reduced in the outcrop region (15° to 30°N). The communication window along $\sigma_\theta = 24.5$ becomes significantly wider compared to the original HR experiment. The sensitivity test of Fig. 2 ) can explain this result. The zonal gradient of the Ekman pumping velocity over the outcrop lines (f_0) becomes weak while the wind stress at the gyre boundary around 10°N (f_d) remains unchanged, and hence the distance

from the ZEPL to the western edge of the communication window at the outcrop latitude increases.

Finally, the effect of reduced winds is examined. According to the analytical solution, the ZMTL approximately bounds the eastern edge of the interior exchange window, as the cyclonic closed gyre appears east of the ZMTL. The distance from the ZEPL to the western edge of the communication window stays the same (Fig. 13c) as expected from the analytical solution, since the ratio of the zonal gradient of Ekman pumping in Eq. (8) at the outcrop and gyre boundary latitudes is unchanged by the weakened wind stress field. However, the eastern edge of the communication window (which is also the eastern edge of the interior exchange window) extends east of the ZMTL.

b. Interior exchange window

The changes, in response to the change of the zonal gradient of Ekman pumping, in the distance between the ZEPL and the western edge of the communication window show a reasonable agreement with the prediction of the analytical calculation. However, the determination of the western and eastern edges of the interior exchange windows involves a more complex analysis. In section 3, it is shown that a larger interior exchange window is created by weak forcing (DSV).

There are two factors that can cause the interior exchange window to extend eastward of the ZMTL. The first possibility is the effect of stratification. Since the ZMTL applies to the vertically integrated transport, the water column may subduct under the ZMTL if the vertically integrated component is not dominant. The second possibility is the existence of a constraint in the equatorial region allowing for more interior pathways from the subtropical gyre. Part of the interior exchange window is inside the equatorial gyre, where ventilation theory and geostrophy may not be applicable. Due to these two possibilities, the results of the numerical experiments for the interior exchange windows will be further analyzed as the analytical calculation does not allow for the second possibility.

We address the first possibility by examining the location of the thermocline ZMTL at the gyre boundary (10°N). The thermocline ZMTL is derived from the model results with the meridional transport stream function [Eq. (5)] being zero. The thermocline ZMTL is around 51°W in the HR experiment, and is moved significantly to the east by switching the wind stress over $0\text{--}20^{\circ}\text{N}$ to the DSV wind stress in experiment 1 (Fig. 14a). This does not occur when the wind stress over $0\text{--}15^{\circ}\text{N}$ remains unchanged in experiment 2 (Fig. 14b). Judging from experiment 1, one might expect that the weakened wind stress causes the ZMTL to move eastward. However, the weakened wind stress in the entire region does not induce the eastward shift of the equatorial thermocline ZMTL in experiment 3 (Fig. 14c), indicating that the effect of the stratification explains only partially why the interior exchange window becomes wider.

Secondly, the possibility of a constraint in the equatorial region is explored. The trajectory analysis suggests a critical latitude at 7°N where the trajectories bifurcate northward or southward (trajectories not shown here). The meridional velocity field at 7°N for each experiment shows two types of sections, one is the DSV type (expt 1, and expt 3), and the other is the HR type (the expt 2; Fig. 15). The difference is whether the velocity fields have two southward velocity cores near 33° and 39°W (expts 1 and 3, Figs. 15a,c) or only one at 39°W (expt 2; Fig. 15b). The two separate cores of southward transport in the DSV-type experiments imply that the vertical profile of the meridional velocity in the equatorial gyre induces more interior pathway water, as seen in the location of the interior exchange pathways marked by crosses in Fig. 15. A reduced wind stress field is also found to bring this separate southward flow close to the DSV type, but it is not clear why these changes in the meridional velocity are produced in the equatorial gyre. However, the result is consistent with what is shown in section 3 that weak forcing creates a wider interior pathways. Due to these changes of the velocity, the interior pathways become more dominant.

The exchange transports carried by the western boundary and interior exchange windows are now examined again at 10°N . As discussed in section 3, the interior exchange transport is larger for the weaker wind stress (DSV). All the total southward transports (below the mixed layer, “1” in Fig. 16) are reduced with respect to the HR experiment. This is expected, especially in experiment 3 where the overall intensity of the wind stress is reduced. Experiments 1 and 2 provide a larger ratio of the interior exchange transport to the total. The ratio of the interior versus western boundary exchange transport increases from $1/5$ in HR (Fig. 16a), to $1/2$ in experiment 1 (Fig. 16b), and to $1/3$ in experiments 2 and 3 (Figs. 16c,d).

These results show that the interior exchange transport depends strongly on the wind stress fields. A reduced region of the upward Ekman pumping and a weak zonal gradient of the Ekman pumping velocity (expt 2) in the southern subtropical gyre broadens the interior exchange window, even though the equatorial winds do not change. A reduced wind stress in the entire basin also enhances the interior exchange pathways (expt 3) by changing the meridional velocity profile in the equatorial region.

6. Summary and conclusions

A reduced-gravity model is used to locate regions in the Atlantic circulation where subsurface water communicates from the subtropics to the Tropics. Experiments were conducted with strong and weak wind forcings, Hellerman and Rosenstein (HR) and da Silva (DSV) climatological annual-mean and monthly wind stress forcings. Due to its stronger wind stress in the equatorial region (Fig. 1), the HR experiment has a stronger tropical gyre than the DSV experiment (Fig. 2). Two isopycnal surfaces that bound the equatorial thermocline (Fig. 3) were chosen to describe the subtropical–tropical interaction. There are four such regions in the subtropics. The first is the “recirculation window” in which fluid parcels recirculate within the subtropical gyres. The second is the “western boundary exchange window” in the central subtropics

where subducted particles flow first to the western boundary, then turn equatorward. The third is the “interior exchange window” from which fluid reaches the equator and the EUC in the basin interior far from the western boundary. The final is the “island circulation” that flows equatorward first and eventually goes back (a closed cyclonic circulation) in the eastern part of the basin. The Bernoulli function on these isopycnal surfaces showed streamlines delineating the recirculation/western boundary exchange/interior exchange/island windows (Fig. 4), which also emerge clearly from the trajectory analysis. Comparing the HR and DSV driven experiments, the interior exchange window in the North Atlantic is wider for the weaker wind stress (DSV: Figs. 4 and 5), which is confirmed by releasing trajectories. Not only is the interior exchange window larger in size, but the transport carried by the interior exchange window is larger for weak wind forcing (DSV: Figs. 7 and 8). In the South Atlantic, the interior exchange pathways are similar in route and volume in both the strong and weak forcing experiments. As the South Atlantic continuously supplies water from the subtropics to the tropics, variability in the North Atlantic was the focus of this study.

An examination of the mean field resulting from seasonally varying experiments shows that the general structure in the equatorial region for the annual mean driven cases are similar to that of the annual-averaged structure in the Bernoulli function fields (Fig. 10). Therefore, the steady-state circulations are used to study the effects of wind stress in the North Atlantic, which is shown to control the width of each exchange window.

The North Atlantic circulation is characterized by a closed region with upward Ekman pumping—an “island”—strongly related to the wind stress distribution. On seasonal time scales, the North Atlantic winds fluctuate significantly, allowing subtropical waters to subduct and flow toward the equatorial region during winter, and preventing communication during the summer (Fig. 9).

Capitalizing on this wind stress pattern, the zonal extent of the communication window was described in terms of the distance from the zero Ekman Pumping line by using a two-moving-layer LPS model [Fig. 11 and Eq. (6)], following Liu (1994). In contrast with Liu (1994), the Ekman pumping velocity is here zonally dependent and allows for a region of positive Ekman pumping. This approach enables the prediction of the western edge of the communication window, given the zonal gradient of the Ekman pumping velocity at the outcrop line and the gyre boundary (Fig. 12). This prediction is useful when part of the wind stress is changed and when the entire communication window is examined, such as in the reduced gravity GCM experiment 2 (Fig. 13b) where the zonal gradient of Ekman pumping velocity along the outcrop line is reduced.

Although it is likely that the subtropical water maintains its properties when it flows along the interior exchange pathways, the western boundary and interior pathways are not distinguishable from the analytical calculation. Therefore, mechanisms that control the interior pathway were further investigated using the reduced gravity GCM. Two effects contribute to the extent of the interior exchange window: one is stratification (seen in and Fig. 14a) in which the cyclonic circulation is closed to the east of what we expect from the barotropic circulation (zero transport stream function evaluated from the wind stress). In this case, the pathway of the thermocline water takes an eastward route. The second is also a stratification effect, but in the equatorial gyre where two cores of meridional velocity appear (7°N). Comparing the meridional velocity fields (Fig. 15), a separate core of southward transport appears in addition to the main southward transport close to the western boundary when winds are reduced. An examination of the transport at 10°N also confirms that the ratio of interior transport is increased relative to the western boundary transport.

The “island” circulation is characterized by upward Ekman pumping velocity, hence smaller layer thickness between layers (high potential vorticity). Therefore, subducted water cannot cross the region to conserve potential vorticity. This is consistent with the “high potential barrier” idea first proposed by Lu and McCreary (1995) and with a North Pacific experiment carried out with our same model (Rothstein et al. 1998). On the other hand, the subtropical–tropical exchange waters are characterized by relatively low potential vorticity. Kubokawa and Inui (1999) found that the minimum potential vorticity waters (i.e., water columns with larger thickness), subducted in the subtropical region, have a strong impact on the lower latitude thermocline structure. Inui et al. (1999) suggest that a sudden intensification of the westerly winds cause the position of minimum potential vorticity water to move westward, which leads to decadal variability in the low latitude ocean. This mechanism is further confirmed by an OGCM experiment in the Pacific (Xie et al. 2000). Therefore, it is very important to investigate exchange windows in the Atlantic, as they have a significant effect on the thermocline structure at low latitudes.

Potential vorticity fields were examined to determine whether the interior exchange pathways water has a specific character, such as minimum potential vorticity or extreme horizontal gradients of potential vorticity. However, no significant potential vorticity characteristics were noted, partly because the mixed layer depth is approximately parallel to the flow, so the horizontal gradient of potential vorticity decreases monotonically westward of the “island.” We also considered the SST and thermocline variability of the equatorial region with respect to the wind stress in the extratropics (using expts 1, 2, and 3) to determine if broadened interior exchange windows cause more changes in the temperature field. However, no systematic relations were found. We speculate that the monotonically decreasing westward mixed layer depth along the outcrop lines that bound the equatorial thermocline may explain the lack of significant difference in temperature between the experiments (expts 1, 2, and 3) in this study. An interannual experiment should allow us to determine if there are situations when the mixed layer along the outcrop lines has a maximum/minimum, but this experiment is beyond the scope of the present investigation.

We did not implement an idealized tracer in this study. The tritium subsurface maximum in the equatorial Pacific (Fine et al. 1981; Fine 1987) suggests the existence of an interior pathway. On the other hand, the tritium distribution in the Atlantic subtropical–tropical circulation does not clearly show a shallow subduction pathway. Heat capacity analysis does not imply a

propagation of the equatorial region (Tanimoto and Xie 2000, personal communication). These issues should be clarified with modeling and observations, as what we have shown in this study is aimed to estimate the water mass transport and communication windows between the subtropics and Tropics.

Acknowledgments

During the course of this study, Ragu Murtugudde, Rui-Xin Huang, Joe Pedlosky, Zhengyu Liu, Shan-Ping Xie, David Walsh, and Masami Nonaka have provided invaluable comments. We would also like to thank people at the Goddard Space Flight Center for helping us set up the model and giving us some useful suggestions. Detailed comments from three anonymous reviewers and the editor were very helpful in improving the paper. This work was supported under NASA Contract NAG5-7194 at MIT (Tomoko Inui and P. Malanotte-Rizzoli) and NASA 622-48-02 at Goddard Space Flight Center (Alban Lazar and Antonio Busalacchi)

REFERENCES

- Blanke B., and S. Raynaud, 1997: Kinematics of the Pacific Equatorial Undercurrent: An Eulerian and Lagrangian approach from GCM results. *J. Phys. Oceanogr.*, **27**, 1038–1053. [Find this article online](#)
- Blanke B., M. Arhan, G. Madec, and S. Roche, 1999: Warm water paths in the equatorial Atlantic as diagnosed with a general circulation model. *J. Phys. Oceanogr.*, **29**, 2753–2768. [Find this article online](#)
- Butt J., and E. Lindstrom, 1994: Currents off east coast of New Ireland, Papua-New Guinea, and their relevance to regional undercurrents in the western equatorial Pacific Ocean. *J. Geophys. Res.*, **99**, 12503–12514. [Find this article online](#)
- Chen D., A. Busalacchi, and L. Rothstein, 1994: The roles of vertical mixing, solar radiation, and wind stress in a model simulation of the sea surface temperature seasonal cycle in the tropical Pacific Ocean. *J. Geophys. Res.*, **99**, 20345–20359. [Find this article online](#)
- Cushman-Roisin B., 1987: Subduction. *Dynamics of the oceanic surface mixed layer: Proc. Aha Huliko'a Hawaiian Winter Workshop*, Honolulu, HI, University of Hawaii at Manoa, 181–196.
- da Silva A., A. C. Young, and S. Levitus, 1994: *Algorithms and Procedures. Atlas of Surface Marine Data*. Vol. 1, 1994, NOAA Atlas NESDIS 6, 83 pp.
- Düing W., R. L. Molinari, and J. C. Swallow, 1980: Somali current: Evolution of surface flow. *Science*, **209**, 588–590. [Find this article online](#)
- Fine R. A., 1987: The penetration of tritium into the tropical Pacific. *J. Phys. Oceanogr.*, **17**, 553–564. [Find this article online](#)
- Fine R. A., J. L. Reid, and H. G. Ostlund, 1981: Circulation of tritium in the Pacific Ocean. *J. Phys. Oceanogr.*, **11**, 3–4. [Find this article online](#)
- Frantantoni D. M., 1996: On the pathways and mechanisms of upper-ocean transport in the tropical Atlantic Ocean. Ph.D. thesis, University of Miami, RSMAS Tech. Rep. 96-006, 247 pp.
- Frantantoni D. M., W. E. Johns, T. L. Townsend, and H. E. Hurlburt, 2000: Low-latitude circulation and mass transport pathways in a model of the tropical Atlantic Ocean. *J. Phys. Oceanogr.*, **30**, 1944–1966. [Find this article online](#)
- Gent P., and M. A. Cane, 1989: A reduced gravity, primitive equation model of the upper equatorial ocean. *J. Comput. Phys.*, **81**, 444–480. [Find this article online](#)
- Harper S., 2000: Thermocline ventilation and pathways of tropical–subtropical water mass exchange. *Tellus*, **52A**, 330–345. [Find this article online](#)
- Hellerman S., and M. Rosenstein, 1983: Normal monthly wind stress over the world ocean with error estimates. *J. Phys. Oceanogr.*, **13**, 1093–1104. [Find this article online](#)
- Huang R. X., 1993: Real freshwater flux as a natural boundary condition for salinity balance and thermohaline circulation forced by evaporation and precipitation. *J. Phys. Oceanogr.*, **23**, 2428–2446. [Find this article online](#)
- Huang R. X., and Q. Wang, 2001: Interior communication from the subtropical to the tropical oceans. *J. Phys. Oceanogr.*, **31**, 3538–3550. [Find this article online](#)
- Inui T., K. Takeuchi, and K. Hanawa, 1999: A numerical investigation of the subduction process in response to an abrupt intensification of the Westerlies. *J. Phys. Oceanogr.*, **29**, 1993–2015. [Find this article online](#)
- Johns W., D. Zhang, and M. McPhaden, 2001: Subtropical cell pathways in the Atlantic inferred from climatological hydrographic data. CLIVAR Workshop on Shallow Tropical and Subtropical Overturning Cells, WCRP Informal Report, No. 4. 182 pp.
- Kraus E., and J. Turner, 1967: A one-dimensional of the seasonal thermocline, II. *Tellus*, **19**, 98–105. [Find this article online](#)

- Kubokawa A., and T. Inui, 1999: Subtropical counter current in an idealized GCM. *J. Phys. Oceanogr.*, **29**, 1303–1313. [Find this article online](#)
- Lazar A., T. Inui, A. J. Busalacchi, P. Malanotte-Rizzoli, and L. Wang, 2001a: Seasonality of the ventilation of the tropical Atlantic thermocline. *J. Geophys. Res.*, in press.
- Lazar A., R. Murtugudde, and A. J. Busalacchi, 2001b: A model study of the propagation of temperature anomalies from subtropics to Tropics within the southern Atlantic thermocline. *Geophys. Res. Lett.*, **28**, 1271–1274. [Find this article online](#)
- Levitus S., 1982: *Climatological Atlas of the World Ocean*. NOAA Prof. Paper 13, 173 pp. and 17 microfiche.
- Lindstrom E., R. Lukas, R. Fine, E. Firing, S. Godfrey, G. Meyers, and M. Tsuchiya, 1987: The western equatorial Pacific ocean circulation study. *Nature*, **330**, 533–537. [Find this article online](#)
- Liu Z., 1994: A simple model of the mass exchange between the subtropical and tropical ocean. *J. Phys. Oceanogr.*, **24**, 1153–1165. [Find this article online](#)
- Liu Z., and S. G. H. Philander, 1995: How different wind stress patterns affect the tropical–subtropical circulations of the upper ocean. *J. Phys. Oceanogr.*, **25**, 449–462. [Find this article online](#)
- Liu Z., and R. C. Pakanowski, 1994: A GCM study of tropical–subtropical upper-ocean water exchange. *J. Phys. Oceanogr.*, **24**, 2606–2623. [Find this article online](#)
- Lu P., and J. P. McCreary, 1995: Influence of the ITCZ on the flow of thermocline water from the subtropical to the equatorial Pacific Ocean. *J. Phys. Oceanogr.*, **25**, 3076–3088. [Find this article online](#)
- Lu P., and B. A. Klinger, 1998: Meridional circulation cells and the source waters of the Pacific Equatorial Undercurrent. *J. Phys. Oceanogr.*, **28**, 62–84. [Find this article online](#)
- Luyten J., J. Pedlosky, and H. Stommel, 1983: The ventilated thermocline. *J. Phys. Oceanogr.*, **13**, 292–309. [Find this article online](#)
- Malanotte-Rizzoli P., K. Hedstrom, H. Arango, and D. Haidvogel, 2000: Water mass pathways between the subtropical and tropical ocean in a climatological simulation of the North Atlantic ocean circulation. *Dyn. Atmos. Oceans.*, **32**, 331–371. [Find this article online](#)
- McCreary J. P., and P. Lu, 1994: On the interaction between the subtropical and equatorial ocean circulation: Subtropical cell. *J. Phys. Oceanogr.*, **24**, 466–497. [Find this article online](#)
- Metcalf W. G., and M. Stalcup, 1967: Origins of the Atlantic Equatorial Undercurrent. *J. Geophys. Res.*, **72**, 4959–4975. [Find this article online](#)
- Murtugudde R., and A. Busalacchi, 1998: Salinity effects in a tropical ocean model. *J. Geophys. Res.*, **103**, 3283–3300. [Find this article online](#)
- Murtugudde R., R. Seager, and A. Busalacchi, 1996: Simulation of the tropical oceans with an ocean GCM couple of an atmospheric mixed layer model. *J. Climate*, **9**, 1795–1815. [Find this article online](#)
- Oberhuber J., 1988: An atlas based on “COADS” data set: The budgets of heat, buoyancy, and turbulent kinetic energy at the surface of the global ocean. Max-Planck-Institute fur Meteorologie Rep. 15, 20 pp.
- Pedlosky J., 1987: An inertial theory of the equatorial undercurrent. *J. Phys. Oceanogr.*, **17**, 1978–1985. [Find this article online](#)
- Price J., R. Weller, and R. Pinkel, 1986: Diurnal cycle: Observations and models of the upper ocean response to diurnal heating, cooling, and wind mixing. *J. Geophys. Res.*, **91**, 8411–8427. [Find this article online](#)
- Rothstein L. M., R.-H. Zhang, A. J. Busalacchi, and D. Chen, 1998: A numerical simulation of the mean water pathways in the subtropical and tropical Pacific Ocean. *J. Phys. Oceanogr.*, **28**, 322–343. [Find this article online](#)
- Seager R., B. Blumenthal, and Y. Kushnir, 1995: An advective atmospheric mixed layer model for ocean modeling purposes: Global simulation of surface heat fluxes. *J. Climate*, **8**, 1951–1964. [Find this article online](#)
- Tsuchiya M., 1981: The origin of the Pacific equatorial 13°C water. *J. Phys. Oceanogr.*, **11**, 794–812. [Find this article online](#)
- Tsuchiya M., R. Lukas, R. A. Fine, and E. Lindstrom, 1989: Source waters of the Pacific equatorial undercurrent. *Progress in Oceanography*, Vol. 23, Pergamon, 101–147.
- Welander P., 1971: Some exact solutions to the equation describing an ideal-fluid thermocline. *J. Mar. Res.*, **29**, 60–68. [Find this article online](#)
- Wilson W. D., E. Johns, and R. L. Molinari, 1994: Upper layer circulation in the western tropical North Atlantic ocean during August, 1989. *J. Geophys. Res.*, **99**, 22513–22523. [Find this article online](#)
- Wyrtki K., 1975: Fluctuations in the dynamic topography in the Pacific Ocean. *J. Phys. Oceanogr.*, **5**, 450–459. [Find this article online](#)

APPENDIX

7. The Thermocline Equations

The 2.5-layer model is shown in [Fig. 11](#). Layer 1 is at the top and layer 2 is underneath the layer 1. Pressure fields are written as

$$P_2 = \gamma_2 h \quad (\text{A1})$$

$$P_1 = \gamma_2 h + \gamma_1 h_1, \quad (\text{A2})$$

where

$$\gamma_n = g(\rho_{n+1} - \rho_n), \quad n = 1, 2 \quad (\text{A3})$$

$$h = h_1 + h_2. \quad (\text{A4})$$

The Sverdrup relation is

$$h^2 + \frac{\gamma_1}{\gamma_2} h_1^2 = D(x, f) + H_0^2 \quad (\text{A5})$$

for the two-moving-layer region, and

$$h^2 = D(x, f) + H_0^2 \quad (\text{A6})$$

for the one-moving-layer region, where $D(x, f)$ is the zonal integral of the Ekman pumping velocity W_e :

$$D(x, f) = \frac{2f^2}{\beta\gamma_2} \int_x^{x_e} W_e dx \quad (\text{A7})$$

Normally x_e is defined by the eastern boundary. However, x_e is the $X_{\psi} = 0$ curve when there is a region of positive Ekman pumping velocity:

$$\int_{X_{\psi}}^{x_e} W_e dx = 0 \quad (\text{A8})$$

Total layer depth H_0 at the outcrop line and at the eastern boundary should be the same as the depth at the outcrop line at $X_{\psi} = 0$, which can be proven by setting

$$D(X_{\psi}, f_0) = 0 \quad (\text{A9})$$

in [Eq. \(A6\)](#).

In the region with two moving layers, the streamline of layer 2 is derived by the Sverdrup relation [[Eq. \(A5\)](#)] and the conservation of potential vorticity below:

$$q_2 = \frac{f}{h_2} = \frac{f_0}{h}, \quad (\text{A10})$$

where $h = h_2 + h_1 = h_2$ at the outcrop line f_0 . Now, the potential vorticity of the layer 2 q_2 is written in terms of total

layer depth h instead of using two variables f and h_2 —simply, the isoline of h is the stream line of layer 2. In order to obtain the equation for h , using the conservation of the potential vorticity in (A10), each layer thickness is

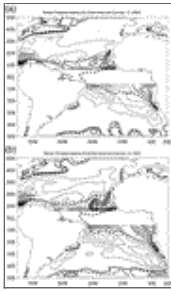
$$h_2 = \frac{f}{f_0}h, \quad h_1 = h - h_2 = \left(1 - \frac{f}{f_0}\right)h, \quad (\text{A11})$$

which are substituted into the Sverdrup equation in the two-moving-layer version (A5). Then, the total layer depth is

$$h^2 = \frac{D(x, f) + H_0^2}{1 + (1 - f/f_0)^2 \gamma_1/\gamma_2}. \quad (\text{A12})$$

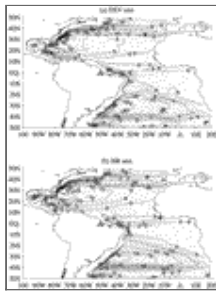
In this particular study, the conservation of potential vorticity is applied for the western boundary through the X_ψ , which is defined by $D(X_\psi, f) = 0$, because the Ekman pumping is positive in the easternmost region of the basin where only a single layer is moving.

Figures



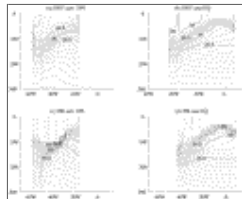
[Click on thumbnail for full-sized image.](#)

FIG. 1. Ekman pumping velocity (the region between 5°N and 5°S is not shown) and $\nabla \times \tau = 0$ lines calculated from the annual mean wind stress data for (a) da Silva (DSV) and (b) HELLERMAN and ROSENSTEIN (HR). Dashed lines indicate $\nabla \times \tau = 0$ line. Black (gray) lines indicate positive (negative) Ekman pumping with a contour interval of $0.5 \times 10^{-4} \text{ cm s}^{-1}$. In North Atlantic low latitudes, Ekman pumping is stronger in HR than in DSV



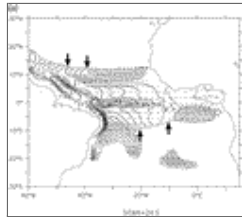
[Click on thumbnail for full-sized image.](#)

FIG. 2. Vertically integrated mean annual transport stream function ψ between the mixed layer and the bottom of the thermocline for (a) weak forcing (DSV) and (b) strong forcing (HR). The contour interval is 1.0 Sv. The equatorial gyre in the North Atlantic is stronger in HR than in DSV



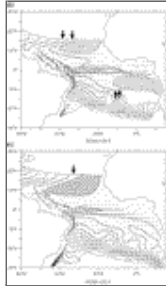
[Click on thumbnail for full-sized image.](#)

FIG. 3. Vertical density profile along (a) 10°N and (b) the equator for the weak forcing (DSV) experiment, (c) 10°N , and (d) the equator for the strong forcing (HR) experiment, with an interval of $0.1 \sigma_\theta$.



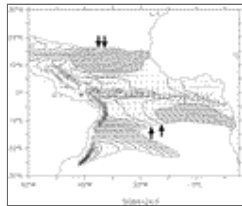
[Click on thumbnail for full-sized image.](#)

FIG. 4. Bernoulli function and current vectors on the $\sigma_\theta =$ (a) 24.5, (b) 25.0, and (c) 25.5 isopycnal surfaces with an interval of 0.1 m (Bernoulli function) for the weak forcing (DSV) experiment. The shaded region indicates the “island” region, which becomes larger at depth and prevents communication between the subtropics and Tropics. The interior exchange windows are marked with arrows




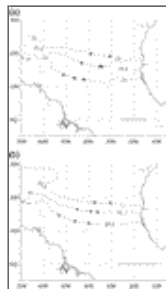
[Click on thumbnail for full-sized image.](#)

FIG. 4. (Continued)



[Click on thumbnail for full-sized image.](#)

FIG. 5. Same as [Fig. 4](#) , except on $\sigma_\theta = 24.5$ for the strong forcing (HR) experiment



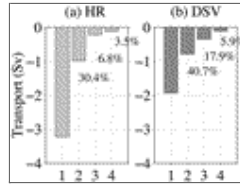
[Click on thumbnail for full-sized image.](#)

FIG. 6. Locations of the communication window and its final position along the equator (+). The boundary between the recirculation (x) and the western boundary exchange windows and the interior window (O) are shown on (a) $\sigma_\theta = 24.0, 24.5,$ and 25.0 for strong forcing (HR) and (b) $\sigma_\theta = 24.5, 25.0,$ and 25.5 for weak forcing (DSV). Dashed lines indicate outcrops



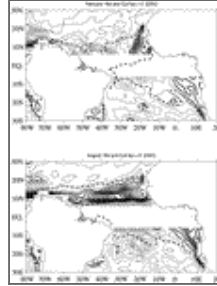
[Click on thumbnail for full-sized image.](#)

FIG. 7. Annual subduction rate S_{ann} (m yr^{-1}) into the main thermocline from the mixed layer for the strong forcing HR experiment. Positive values indicate subduction, and negative values indicate entrainment



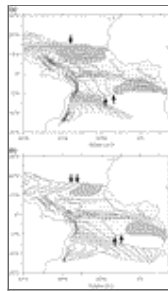
Click on thumbnail for full-sized image.

FIG. 8. Transport at 10°N for each exchange window in the strong forcing (HR) experiment: 1) the total southward transport below the mixed layer, 2) southward transport within the thermocline layer carried by the western boundary communication window, 3) interior window, and 4) “island circulation.” Listed percentage is the ratio of each transport to the total southward transport: (b) same as (a) but for the weak forcing (DSV) experiment



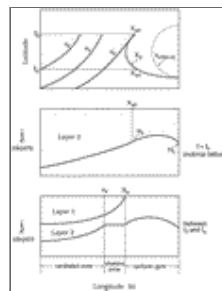
Click on thumbnail for full-sized image.

FIG. 9. Ekman pumping velocity and $\nabla \times \tau = 0$ lines calculated from the climatological data for da Silva from (a) Feb and (b) Aug. Black dashed lines indicate $\nabla \times \tau = 0$ lines. Black (gray) lines indicate positive (negative) Ekman pumping with a contour interval of $0.5 \times 10^{-4} \text{ cm s}^{-1}$



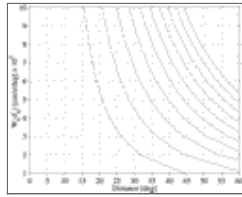
Click on thumbnail for full-sized image.

FIG. 10. Bernoulli function from the mean of seasonally varying experiments and current vectors superimposed on (a) $\sigma_\theta = 24.5$ for the strong forcing (HR) experiment and (b) $\sigma_\theta = 25.0$ for the weak forcing (DSV) experiment, with a contour interval of 0.1 m. Notations are the same as [Fig. 4](#)



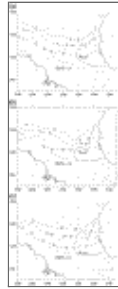
Click on thumbnail for full-sized image.

FIG. 11. Schematic of the flow of the ventilated layer in a two-moving-layer model. The upper figure is the horizontal view x_2 : boundary between recirculation and western boundary communication regions, x_3 : boundary between western boundary and interior communication windows, x_4 : shadow zone boundary, and x_c : the zero Ekman pumping line; f_0 is the outcrop latitude. The middle figure is a vertical section of the density structure along the latitude $f = f_0$, the lower figure is the vertical section along a latitude between $\vec{f} = f_0$ and f_d



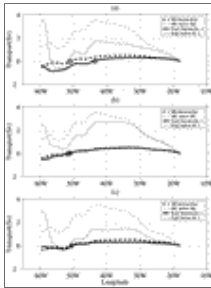
[Click on thumbnail for full-sized image.](#)

FIG. 12. Sensitivity of the width of the communication window to the zonal gradient of the Ekman pumping, based on the analytical calculation. The zonal gradient of the Ekman pumping is divided into 10 levels between 1.0 and $1.0 \times 10^{-4} \text{ cm s}^{-1}/\text{deg}$ both at the outcrop line and the gyre boundary latitudes. The y axis represents the intensity of the zonal gradient of the Ekman pumping along the outcrop line, and the x axis represents the distance (degrees) of the western edge of the communication window (x_2) from the zero Ekman pumping velocity line. Different lines indicate that the zonal gradient of Ekman pumping at the gyre boundary is increasing (from left to right)



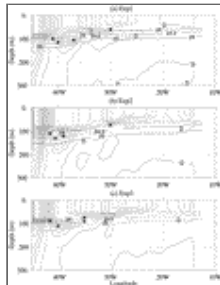
[Click on thumbnail for full-sized image.](#)

FIG. 13. The communication windows: as in Fig. 6 but for (a) expt 1, (b) expt 2, and (c) expt 3. Gray lines are zero meridional transport stream function lines (ZMTL) (calculated from the wind stress data by integrating the Ekman pumping velocity from the eastern end of the basin), and solid lines indicates the zero Ekman pumping velocity line ($We = 0$)



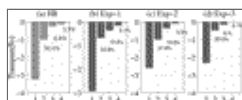
[Click on thumbnail for full-sized image.](#)

FIG. 14. The meridional transport stream function ψ calculated at 10°N (choke latitude) for (a) expt 1, (b) expt 2, (c) expt 3. (Thin line is for the layer beneath the mixed layer to the bottom layer, thick line is for the thermocline layer.) The region to the east of the circles ($\psi = 0$) has a closed circulation



[Click on thumbnail for full-sized image.](#)

FIG. 15. Meridional velocity at 7°N for (a) expt 1, (b) expt 2, (c) expt 3 with the isopycnal surfaces superimposed. Lines with light shading indicate northward velocities and dark shading indicate southward velocities. The black solid lines are the isopycnal lines. Contour interval for the velocity is 0.05 cm s^{-1} . The interior exchange windows at 7°N are indicated with \times for each experiment



[Click on thumbnail for full-sized image.](#)

Corresponding author address: Dr. Tomoko Inui, International Arctic Research Center, University of Alaska, 930 Koyukuk Dr., Fairbanks, AK 99775-7335. E-mail: tomoko@iarc.uaf.edu

[top ▲](#)



© 2008 American Meteorological Society [Privacy Policy and Disclaimer](#)

Headquarters: 45 Beacon Street Boston, MA 02108-3693

DC Office: 1120 G Street, NW, Suite 800 Washington DC, 20005-3826

amsinfo@ametsoc.org Phone: 617-227-2425 Fax: 617-742-8718

[Allen Press, Inc.](#) assists in the online publication of AMS journals.